sustainability

MDPI

Article

Investigation on the Potential of Various Biomass Waste for the Synthesis of Carbon Material for Energy Storage Application

Brenda Ai-Lian Lim [1,2,*], Steven Lim [1,2,*], Yean Ling Pang [1,2], Siew Hoong Shuit [1,2], Kam Huei Wong [1,2] and Jong Boon Ooi [3]

[1] Department of Chemical Engineering, Lee Kong Chian Faculty of Engineering and Science, Universiti Tunku Abdul Rahman (UTAR), Jalan Sungai Long, Kajang 43000, Malaysia; pangyl@utar.edu.my (Y.L.P.); shuitsh@utar.edu.my (S.H.S.); wongkh@utar.edu.my (K.H.W.)
[2] Centre of Photonics and Advanced Material Research, Universiti Tunku Abdul Rahman (UTAR), Bandar Sungai Long, Kajang 43000, Malaysia
[3] Mechanical Engineering Discipline, School of Engineering, Monash University Malaysia, Jalan Lagoon Selatan, Bandar Sunway, Subang Jaya 47500, Malaysia; ooi.jongboon@monash.edu
* Correspondence: brendalim2707@1utar.my (B.A.-L.L.); stevenlim@utar.edu.my (S.L.)

Abstract: The metal–air battery (MAB) has been a promising technology to store energy, with its outstanding energy density, as well as safety features. Yet, the current material used as air cathode is costly and not easily available. This study investigated a few biomass wastes with good potential, including the oil palm empty fruit bunch and garlic peel, as well as the oil palm frond, to determine a sufficiently environmentally-safe, yet efficient, precursor to produce carbon material as an electro-catalyst for MAB. The precursors were carbonized at different temperatures (450, 600, and 700 °C) and time (30, 45, and 60 min) followed by chemical (KOH) activation to synthesize the carbon material. The synthesized materials were subsequently studied through chemical, as well as physical characterization. It was found that PF presented superior tunability that can improve electrical conductivity, due to its ability to produce amorphous carbon particles with a smaller size, consisting of hierarchical porous structure, along with a higher specific surface area of up to 777.62 m^2g^{-1}, when carbonized at 600 °C for 60 min. This paper identified that PF has the potential as a sustainable and cost-efficient alternative to carbon nanotube (CNT) as an electro-catalyst for energy storage application, such as MAB.

Keywords: metal–air battery; carbon particles; biomass waste; electro-catalyst

Citation: Lim, B.A.-L.; Lim, S.; Pang, Y.L.; Shuit, S.H.; Wong, K.H.; Ooi, J.B. Investigation on the Potential of Various Biomass Waste for the Synthesis of Carbon Material for Energy Storage Application. *Sustainability* **2022**, *14*, 2919. https://doi.org/10.3390/su14052919

Academic Editor: Thanikanti Sudhakar Babu

Received: 30 December 2021
Accepted: 9 February 2022
Published: 2 March 2022

1. Introduction

Energy sources that are renewable have gradually developed and been implemented to compensate for the decreasing and non-environmentally safe sources, which are mainly fossil fuel derivatives [1]. With the advanced development in science and technology, metal–air batteries (MAB) are manufactured as devices to store energy from the unstable renewable yet green energy source that depend primarily on the surrounding nature, including the weather that affects the availability of the sun, wind, and water currents. Currently, energy storage technologies are used to store energy in many off grid devices, such as electrical automobiles, hand phones, power banks, laptops, and many other household appliances [2]. The conventional energy storage technology, which is commonly known as the lithium-ion battery (LiB), has been generally established, while being commonly used in the industry. Nonetheless, the LiB possessed its own drawbacks, which includes slow charging time, bulky in size, and safety concerns, such as electrolyte leakage and flammable components, as well as had approached its theoretical energy density and recyclability limit [3]. The first metal–air battery was created back in the year 1800, and continuous research had been carried out to improve the efficiency and affordability of the device [4]. The MAB was generally design with primary components consisting of a cathode, an anode, and a

liquid or non-liquid electrolyte. It works through the electrochemical reactions that take place among the components, whereby the atmospheric oxygen is reduced, and the metal electrode is oxidized, which assembles into reversible metal-oxides [5]. An advantage to MAB is the application of a half-open system, which can facilitate the oxygen reduction reaction (ORR) that takes place at the cathode [5]. The open structure allows a substantial size and weight reduction of the battery [6]. MAB is applicable in the storage of any intermittent energy created from renewable energy sources, including hydropower, as well as geothermal power, to consistently maintain continuously energy supply. MAB has shown great potential for a device to store energy, with its high theoretical energy density (as much as 5928 Wh kg^{-1}), improved recyclability, and light and compact design, compared to LiBs [6,7]. However, the MAB technology is still lacking, in terms of economics, endurance, and efficiency, which affects the status of commercialization of the device.

Many researchers came to understand that majority of the chemical and physical properties of the air cathode material had a large impact on the capability of a MAB [5,8]. According to Ha et al., the catalytic efficiency of the battery can be controlled with the properties of the air cathode, as the charge and discharge reactions relies on the availability of active sites to store discharge products, as well as the diffusion pathway [9]. The commercial material used to fabricate the air cathode that is used for MAB includes rare metals, such as the Pt-based materials, RuO_2, and IrO_2 [10]. These rare metal materials are not economical, less stable, and are inclined to capitulate, due to poisoning from methanol, as well as carbon dioxide. There are researchers who had also disclosed that carbon-based materials contained advantageous characteristics that give them greater suitability as precursors to synthesize electro-catalyst in MABs, due to its highly porous structure [11]. Carbon nanotubes (CNTs) were utilized as an electro-catalyst material due to its elevated energy density and exceptional cyclic-life [12]. Unfortunately, CNTs are usually very expensive, due to its highly complex production method. To mitigate this issue, researchers had initiated studies to find a suitable carbon material substitute by using biomass wastes as precursors that are more economical and environmentally friendly.

Biomass wastes are typically generated from redundant plants or animal parts found in industrial, agricultural, and municipal waste. They are primarily made of carbohydrates and polysaccharides, which provides high content of carbon, oxygen, and hydrogen atoms, as well as less significant components [13]. The unique and natural composition found in biomass wastes rendered them as a competent, yet sustainable, precursor material to produce carbon material. Besides, the natural availability of other components, including silicon and nitrogen, increases the possibility for self-heteroatom doping to occur [14]. Heteroatom doping was found to be able to improve the electrochemical efficiency of the electro-catalyst material by altering its chemical and physical structures, thus improving the electrical conductivity, surface wettability, and transfer of charges of the battery [15]. Currently, a large amount of biomass wastes were being created globally, which presented a huge threat to the environment if not being disposed properly. The usage of biomass waste as precursor material to produce of carbon material can not only reduce the waste accumulation, but also acted as a substitute for higher cost products. Different biomass wastes can produce carbon materials with different properties with their unique structures, as well as elemental and lignocellulosic compositions [16]. Due to this, the study of carbon material from biomass waste will be vital to synthesize a high performing electro-catalyst for energy storage applications, such as MAB.

Lignocellulosic components found in biomass wastes are bonded by covalent and non-covalent bonding [17]. The carbonization of lignocellulosic biomass wastes produces carbon materials with hierarchical pores which is a mixture of different pore size ranging from micropores to macropores. Hierarchical porous structures provide greater specific surface area and plenty of diffusion channels that can improve the electrochemical reactions that takes place at the cathode of the battery [18]. Each lignocellulosic component, including lignin, cellulose, and hemicellulose, decomposes at different temperatures range, as each component has an individual thermal stability, due to the different chemical bondings

present. Hemicellulose is predicted to thermally break down at temperature ranging from 180 to 270 °C, while cellulose is anticipated to disintegrate at 270 to 350 °C [19]. Meanwhile, lignin has a greater structural complexity, whereby it begins to disintegrate only when the temperature exceeds 300 °C.

Various studies have been done on the synthesis of carbon materials for electric storage application from different types of biomass waste with different synthesis methods [20,21]. These studies focused on individual biomass waste as a precursor, while studying the effect of different synthesis parameters, such as the types of doping agent, carbonization temperature, and carbonization method. There were other studies done on multiple biomass wastes, and these studies focused mainly on the effect of heteroatom content [22] on the synthesis methods [16,23] and synthesis parameters [24]. However, there is insufficient information available that focuses on the fundamental relationship between the pyrolysis temperature and time, as well as the composition of the lignocellulosic component in the precursor to synthesize carbon material to be used in metal air batteries. This information is vital when it comes to the selection of suitable precursors and synthesis parameters to synthesize an optimum electro-catalyst for electric storage application.

For this study, there are three individual biomass wastes containing unique properties that were selected as raw materials to synthesize carbon material as electro-catalyst, which were the oil palm empty fruit bunch (EFB) and garlic peel (GP), as well as oil palm frond (PF). These biomass wastes are easily accessible, as Malaysia is presently second to the world largest producer of palm, while garlic is one of the basic cooking ingredients in the country [25]. These biomass wastes were all obtained without any charge. The oil palm frond and garlic peel have no commercial value yet, as these wastes are currently not reused. On the other hand, the oil palm empty fruit bunch is currently reused for other applications, such as the bio-fertilizer, as well as methane production [26,27]. According to Salleh et al., the price of EFB in the year 2018 was c.a. USD 70.85 per ton, which was calculated to be c.a. USD 72.62 per ton in the year 2021, when the CPI inflation rate was taken into consideration [28,29]. EFB, PF, and GP have different elemental and lignocellulosic compositions, as well as surface textures, which can result in the production of carbon materials with different properties. Currently, there are no studies done on these precursors for electrical storage applications in MAB [30,31]. Therefore, this study aimed to identify their feasibility as a suitable raw material to synthesize a carbon material as an electro-catalyst for MAB, based on the chemical and physical characterization tests conducted.

2. Materials and Methods

2.1. Materials

The biomass wastes selected as precursor in this study includes EFB and PF, as well as GP, as shown in Figure 1. EFB, along with PF, were both obtained by car from an oil palm plantation locally found in Tangjung Tualang, Perak on the 3rd of May 2021. On the other hand, the acquisition of GP had been done from a locally based food and beverage factory located within the industrial area of Kampung Baru, Selangor on the 21st of April 2021; 37% concentrated hydrochloric acid (HCl) and 98% potassium hydroxide (KOH) were bought from Merck and Friendemann Schmidt Chemicals, respectively, to synthesize carbon material.

(a) (b) (c)

Figure 1. (**a**) Raw OPEFB; (**b**) raw OPF [32]; (**c**) raw GP.

2.2. Synthesis of Carbon Material

Figure 2 shows the process flow of the production of a carbon material for this study. The biomass waste was first washed multiple times to remove other solid impurities before being placed in the drying oven (Memmert, UNB 100) at a constant temperature of 80 °C for approximately 24 h. After that, the size of the dried precursor was then reduced by grinding and sieving to obtain the size of less than 300 µm and stored in individual sealed containers prior to usage. For the study of the carbonization temperature parameter, the carbonization process of dried precursor was accomplished by filling the crucible with 5.0 g of biomass precursor powder and inserted into a carbolite furnace (Carbolite, RHF 15/8) before setting the carbonization temperature to 450 °C, 600 °C and 700 °C with a carbonization duration of half an hour. On the other hand, the carbonization time was manipulated from 30 to 60 min whereas the carbonization temperature was set constant at 600 °C for the study of carbonization time. Subsequently, the raw material that was carbonized was left to cool overnight, before it underwent activation using the wet chemical impregnation method, whereby the carbonized precursor was infused with activating agent KOH at a 3 to 1 weight ratio (carbon to KOH), and 5 mL of water was added to dissolve the added KOH before being stirred continuously with a magnetic stirrer for 24 h. Then, the slurry was then left to dry in the same oven at a temperature of 80 °C until all the moisture content was removed. The agglomerated dried mixture was ground into fine powder form by using a pestle and mortar before it underwent heat treatment in the carbolite furnace at a temperature 600 °C for 30 min. After the treated carbon material was cooled to room temperature, the carbon material was washed with HCl solution of 1.0 mol concentration in order to rinse off the remaining inorganic salts before further rinsing with distilled water until neutral pH was achieved followed by drying it overnight in the oven. Similarly, the size of the dried agglomerated activated carbon was reduced by grounding using a pestle and mortar to remove agglomeration before being stored in individual sealed containers. Hereupon, activated carbon materials were formed and each of individual samples with unique labels EFB-x-y, GP-x-y, and PF-x-y, by which x described the carbonization temperature, while y represented the carbonization time, which were 30, 45, and 60 min.

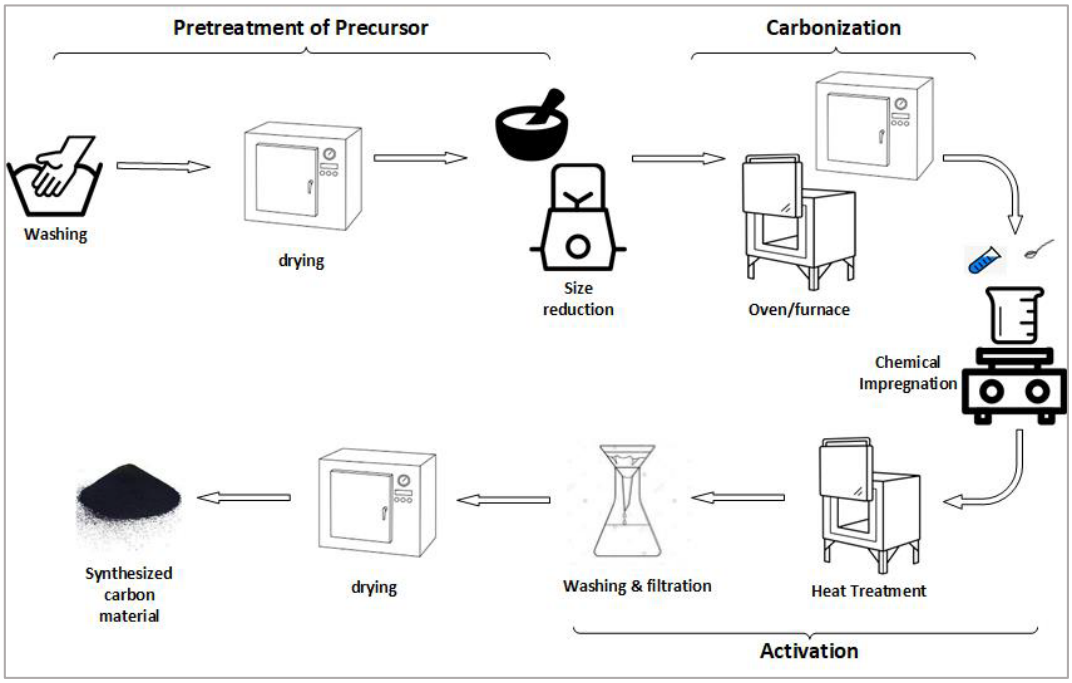

Figure 2. Carbon material synthesis process flow.

2.3. Characterization of Carbon Material

2.3.1. Lignocellulosic Component Test

The extractives were removed from the raw materials using the soxhlet extraction method with methanol as solvent for 4 h and the extractive content were calculated accordingly using Equation (1) [33]. The ash content in the raw precursors were determined in accordance with the procedure by the National Renewable Energy Laboratory [34]. The lignocellulosic component test was carried out in accordance with the Klason for lignin and Tappi T203 cm-09 test method for the determination of the cellulose and hemicellulose components with slight modification [35]. The content percentage were calculated as shown in the equations below.

Extractive content percentage:

$$Extractive\ (\%) = \frac{W_{ex,1} - W_{ex,2}}{W_{ex,1}} \times 100\% \quad (1)$$

Ash content percentage:

$$Ash\ content\ (\%) = \frac{W_{ash,2}}{W_{ash,1}} \times 100\% \quad (2)$$

Lignin content percentage:

$$Lignin\ content\ (\%) = \frac{W_{l,2}}{W_{l,1}} \times 100\% \quad (3)$$

Cellulose and Hemicellulose content percentage:

$$Hemicellulose\ content\ (\%) = \frac{6.85(V_b - V_t) \times 0.2}{V \times 1.5} \times (100 - Lignin\ content)\% \quad (4)$$

$$Cellulose\ content\ (\%) = 100\% - Lignin\ content(\%) - Hemicellulose\ content(\%) \quad (5)$$

where $W_{ex,1}$ represents the weight of the raw dried precursor before extraction while $W_{ex,2}$ indicates the dry weight of extractive-free precursor. $W_{ash,1}$ and $W_{ash,2}$ represent the weight of dried raw precursor before and after carbonization, respectively. $W_{l,1}$ and $W_{l,2}$ constitute for the weight of dried raw precursor and dried extracted lignin, respectively. V_b and V_t constitute for the volume of 0.1 N ferrous ammonium sulfate titrated into the blank solution and sample, respectively, while V indicates the volume of pulp filtrate used in the sample.

2.3.2. Chemical Characterization

The chemical properties of each of the synthesized samples were analyzed using the scanning electron microscopy-energy dispersive X-ray (SEM-EDX) (Hitachi, S-3400 N), thermogravimetric analysis (TGA) (Thermo Scientific Sorptometic, SO1990), and Fourier transform infrared spectroscopy (FTIR) (Nicolet, iS10). The SEM-EDX method was utilized to analyze the presence of elements on the sample surface. Meanwhile, TGA analysis was carried out to observe the weight changes of the raw materials, with temperatures ranging from 30 to 1000 °C at the flow rate of 10 °C min^{-1} in N_2 atmosphere. The weight percentage and derivative weight curves were obtained and studied for the individual raw precursors. FTIR analysis was executed to analyze and compare the presence of the chemical bonds within the wavelength spectrum, ranging from 400 to 4000 cm^{-1}, for the raw materials, along with the selected carbon samples at 700 °C and 30 min.

2.3.3. Physical Characterization

The physical properties of several selected carbon samples synthesized were being characterized through X-ray diffraction (XRD) analysis (Shidmazu, XRD-6000), the Brunauer–Emmet–Teller (BET) surface analysis (Micromeritics, 3Flex), and the field emission scanning electron microscopy (FESEM) (JEOL, JSM-6701F). The XRD analysis had been carried out, with a scan range of 10 to 60 °C, at a scan rate of 2 °C min^{-1}, in order

to study and compare the crystalline characteristics of the raw precursors as well as the selected carbonized precursors. The individual specific surface area (SSA) of each of the carbon samples was verified by carrying out the BET analysis. 0.4 g of each carbon samples were inserted in each tube and left to degass at 150 °C for 6 h to remove moisture content before being purged with N_2 gas to calculate the surface area of the sample based on the adsorption as well as desorption of nitrogen molecules on the sample surface. Meanwhile, FESEM was utilized to analyze the surface morphology of each sample, synthesized with the size of the sample, porous structure, and surface texture at different magnifications of 15, 30, and 50 thousand times.

3. Results and Discussion

3.1. Chemical Properties Characterization

3.1.1. Lignocellulosic Composition Test

The results of the lignocellulosic composition test were tabulated in Table 1. Based on the result obtained, EFB had higher lignin and cellulose content than that of PF and GP. On the other hand, PF had the highest hemicellulose content, as well as lowest lignin and cellulose content, among the three precursors. The remaining dry weight of the precursors accounted for the organic solvent extractives and ash contents.

Table 1. Lignocellulosic component composition of EFB, PF, and GP.

Components (%)	EFB	PF	GP
Extractives	22.55 ± 3.30	31.10 ± 4.88	15.85 ± 0.07
Ash	6.827 ± 0.87	3.71 ± 0.18	3.84 ± 0.05
Lignin	24.67 ± 3.49	17.91 ± 2.11	19.30 ± 3.57
Hemicellulose	14.93 ± 0.20	39.51 ± 0.22	26.62 ± 0.23
Cellulose	40.69 ± 0.20	19.61 ± 0.22	37.68 ± 0.23

The specific surface area of an electro-catalyst material plays a crucial role in the electrochemical efficiency through the active sites that are present for reactions to happen [36]. Rios et al. highlighted that the biomass with high lignin content is more likely to produce carbon materials with a more macroporous structure [37]. Macropores provides diffusion channel for particles, but it also results in lower SSA, as well as the available active sites that could hinder the electrochemical performance of the carbon material. Chen et al. had separated lignin, cellulose, and hemicellulose from corn straw to form carbon material and discovered that hemicellulose provided a higher specific surface area, followed by cellulose [38]. According to Leng et al., high ash content resulted to a lower micropore structure. As the development of a porous structure is linked to the removal of volatile matters and ash, which are non-volatile inorganic residues that cause blockage of the pores and, thus, result in low micropore surfaces that account for the available active sites on the material [39]. Based on the findings above, lower lignin and ash contents, as well as higher hemicellulose content, are preferable to ensure a larger surface area of the carbon material.

3.1.2. SEM-EDX Analysis

Table 2 listed the elemental (C, N, O, S) content found on the surface of the raw biomass precursors and synthesized carbon samples at 600 °C by using SEM-EDX. By comparing the elemental content of the raw biomass precursors and the carbonized biomass precursors, the carbonization of the biomass wastes had resulted in an increase in carbon atomic percentage, as volatile matters were removed at an elevated temperature and, thus, increased the carbon purity of the samples [40]. The increase of carbon content also indicated that the raw material had broken down into carbon. Carbonization of the raw materials also caused a decrease in oxygen content, especially in garlic peel, which justified the FTIR results in the later section. The carbonization process exhibited different effects on the content of N and S heteroatoms for each precursor. The N atom content in EFB increased, while a decrease in the N content was observed for PF and GP. On the other hand,

the S content in EFB and PF decreased, but increased for GP. The change in heteroatoms may be attributed to the interaction between the atoms, as well as free radicals, on the carbon surface, which occurred during the activation process [40].

Table 2. Elemental content of raw materials and synthesized materials at 600 °C with SEM-EDX.

Elements (At %)	Raw OPEFB	EFB-600-30	Raw OPF	PF-600-30	Raw GP	GP-600-30
C	54.16	80.44	53.52	79.11	51.61	86.42
N	1.29	3.07	1.46	1.35	1.63	0.82
O	44.28	16.41	44.85	19.49	46.62	12.60
S	0.26	0.08	0.18	0.05	0.14	0.16

High carbon content is an advantage as carbon possessed good conductivity, tailorable chemical properties, and superior resistance to corrosion [41]. On the other hand, the electrical resistivity of a material is subjected to the impurity present. Kolanowski et al. had reported that an excess in oxygen content might influence the storage of discharge product as it disrupts the surface conjugation of the synthesized carbon material [18]. N and S heteroatoms are common doping agents as they help to elevate the SSA of a carbon material, by means of redistributing the electron charges and alteration of spin density [42,43]. While some impurities can facilitate the electrical conductivity of the material, there are also impurities that can disrupt its conductivity performance.

3.1.3. TGA Analysis

Figure 3 present the weight percentage and derivative weight curves of raw EFB, PF and GP from room temperature to 900 °C by TGA analysis, respectively. It was observed that the derivative weight curve and weight percentage curve for all three samples displayed a small peak and a gradual slope, respectively, within room temperature to 100 °C, which represented the change in sample weight, due to the removal of moisture. Besides that, another sharper peak and sheer slope in the derivative weight curve and weight percentage curves, within the temperatures 200 to 400 °C, were observed, which aligned with the lignocellulosic component decomposition temperatures. The decomposition of lignocellulosic components had resulted in a significant drop in sample weight. The peak and slope, obtained through this characterization method, had confirmed that the lignocellulosic components decomposed within the temperature 200 to 400 °C. Nevertheless, it was observed that PF and GP exhibited a slight individual peak, at approximately 250 °C, which represented decomposition of hemicellulose [44]. This also indicated the higher hemicellulose content present in both precursors, as compared to EFB.

Above 400 °C, the changes in weight were observed to be minimal, as most lignocellulosic components had decomposed and other volatile compounds were removed. Sunphorka et al. reported that the weight change within 400 to 800 °C may be attributed to the slow lignin decomposition, due to its amorphous and highly complex structure [45]. Above 800 °C, the weight percentage curve of EFB, PF and GP exhibited minimal changes with the lowest weight percentage obtained at 6.11%, 8.59%, and 3.57%, respectively. Based on the final weight percentage, it can be concluded that PF had the highest thermal stability, as it was able to preserve more weight at an elevated temperature [46]. A precursor with a good thermal stability is preferred to prevent the loss in porous structure during the synthesis process, which will greatly impact on the availability of active sites, as well as the diffusion channel for the reaction to take place.

3.1.4. FTIR Analysis

Figure 4 displays the results obtained from the FTIR analysis carried out on the raw materials along with the selected carbon samples. It was then discovered that the O-H bond peaks within the wavenumber ranging from 3650 cm^{-1} to 3200 cm^{-1} had flattened tremendously, particularly for GP, whereby it demonstrated a drop in the natural oxygen

content present in the carbonized sample, as shown in Table 2. The peak present at approximately 2900 cm^{-1} for raw GP represented the C-H bond which also flattened after carbonization [47]. Within the wavenumber ranging from 1650 cm^{-1} up to 1560 cm^{-1}, as well as 1260 cm^{-1} up to 1020 cm^{-1}, the presence of C=N double bond and C-N bond, respectively, in the samples indicated that the nitrogen was present in the raw materials which is a potential natural doping agent [48]. Many researchers had concluded that the doping of nitrogen is capable of boosting the SSA of a carbon material synthesized by redistributing the charges and various N arrangements, which enhances the interaction between the carbon and oxygen molecules [42,49]. Within the lower section of the wavenumber range (1035–1149 cm^{-1}), the amount of natural polysaccharides present in the samples were observed to have dropped after the raw materials were carbonized, which confirmed the decomposition of lignocellulosic components. However, it can be seen that the OPEFB after carbonization had a slight peak at 1035–1149 cm^{-1}, as compared to OPF and GP, which may imply that not all polysaccharides, especially lignin, were broken down for OPEFB.

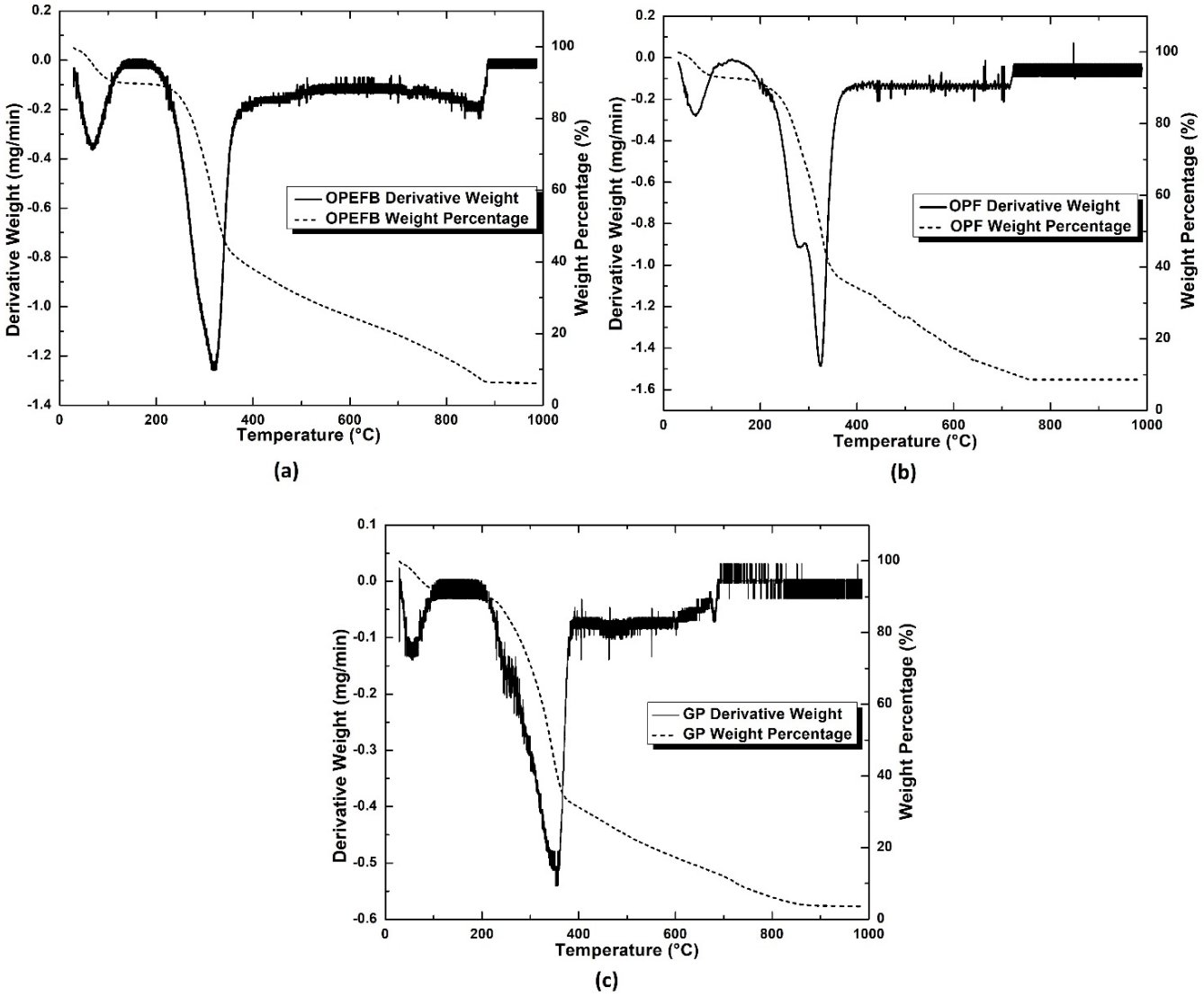

Figure 3. Weight percentage and the derivative weight curve of raw (**a**) EFB, (**b**) PF, and (**c**) GP obtained from TGA analysis.

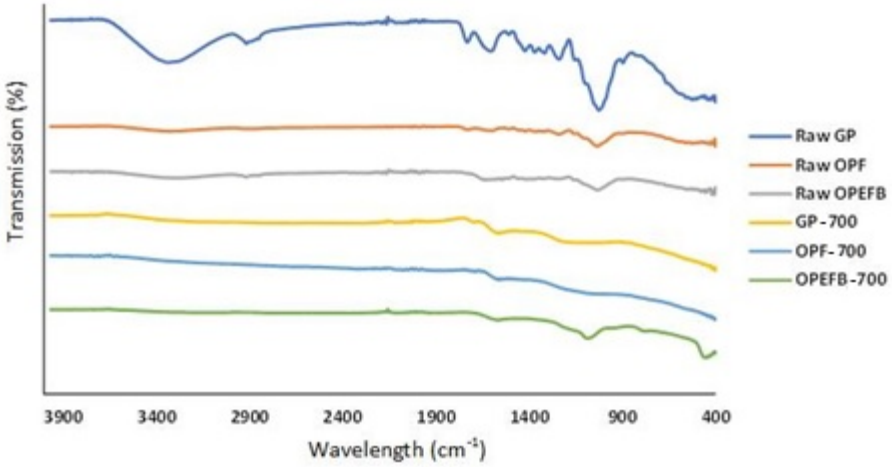

Figure 4. FTIR Spectra of Samples.

3.2. Physical Properties Characterization

3.2.1. XRD Analysis

Figure 5 depicts the XRD peaks for selected samples, which are raw EFB, raw PF, raw GP, EFB-600-30, PF-600-30, and GP-600-30, to compare the crystalline structure of each carbonized biomass precursors. All samples displayed a peak at approximately 21 to 24°, as well as a smaller peak at approximately 44°, which corresponded to the (002) and (100) standard carbon peaks [50]. It was observed that all the carbonized precursors exhibited broader peaks than the raw biomass precursors which implied that carbonization of the biomass precursors resulted in a change in the carbon structure into an amorphous structure. Another observation made was the growth in the peaks at 44 °C after carbonization of all the biomass precursors. However, it can be observed that the peaks at 44 °C for PF is slightly sharper than EFB and GP, which implied that PF may have a small degree of graphitization. According to Chakraborty et al., the extent of graphitization of a carbon material affects its electrical conductivity [51]. The degree of graphitization often increases with carbonization temperature. Bhat et al. had observed that higher the degree of graphitization caused more carbon to be hybridized into sp^2 configuration whereby electrons are more mobile which enhances the electrical conductivity of the material [52]. Hereby, it can be assumed that PF has better potential to produce graphitic carbon materials that is preferable for electrical conductivity.

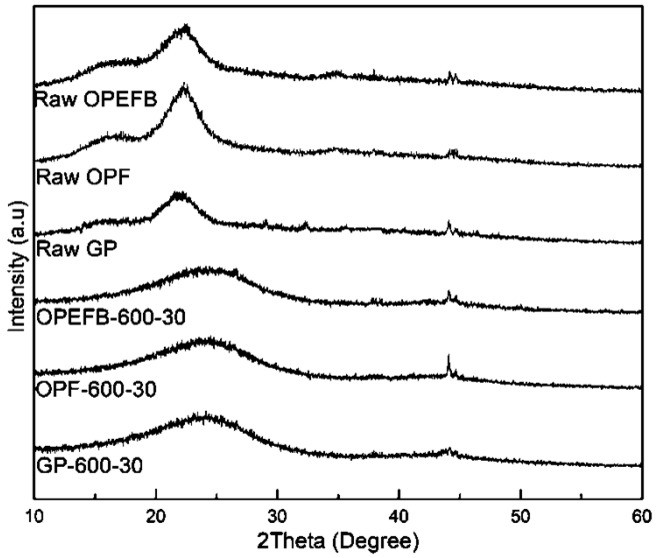

Figure 5. XRD patterns of different biomass samples.

3.2.2. BET Analysis

It was discovered from Figure 6a that increasing the carbonization temperature had caused the BET SSA of both PF and GP raw materials to increase. On the contrary, the specific surface area for EFB had increased insignificantly and then decreased even lower when the carbonization temperature was increased. PF-700-30, in turn, showed better capability in the formation of a higher specific surface area, due to its ability to obtain the greatest specific surface area of 548.26 m^2g^{-1}, when the carbonization temperature was elevated to 700 °C, in comparison with EFB-700-30 and GP-700-30 at 442.02 m^2g^{-1} and 541.01 m^2g^{-1}, respectively. This could be associated to the lignocellulosic components content in the precursors as every component have different disintegrating temperature range. The higher lignin content in EFB (24.7%), compared to PF and GP (17.9% and 19.32%, respectively) could clarify the insignificant changes in the BET SSA for EFB during the increase in carbonization temperature. The considerable rise in SSA of GP, during the rise in temperature of the carbonization process from 450 up to 600 °C could be a result of a greater content in cellulose present in GP that disintegrated at an elevated temperature in comparison to that of hemicellulose. Contrarily, PF had demonstrated a continuous hike in SSA while the temperature of the carbonization process was elevated whereby it may be associated with the greater hemicellulose content along with the decreased cellulose and lignin content in comparison to GP. These results had shown that PF do not depend on such an elevated temperature to break down and hence, it was able to obtain the highest BET SSA at 600 and 700 °C.

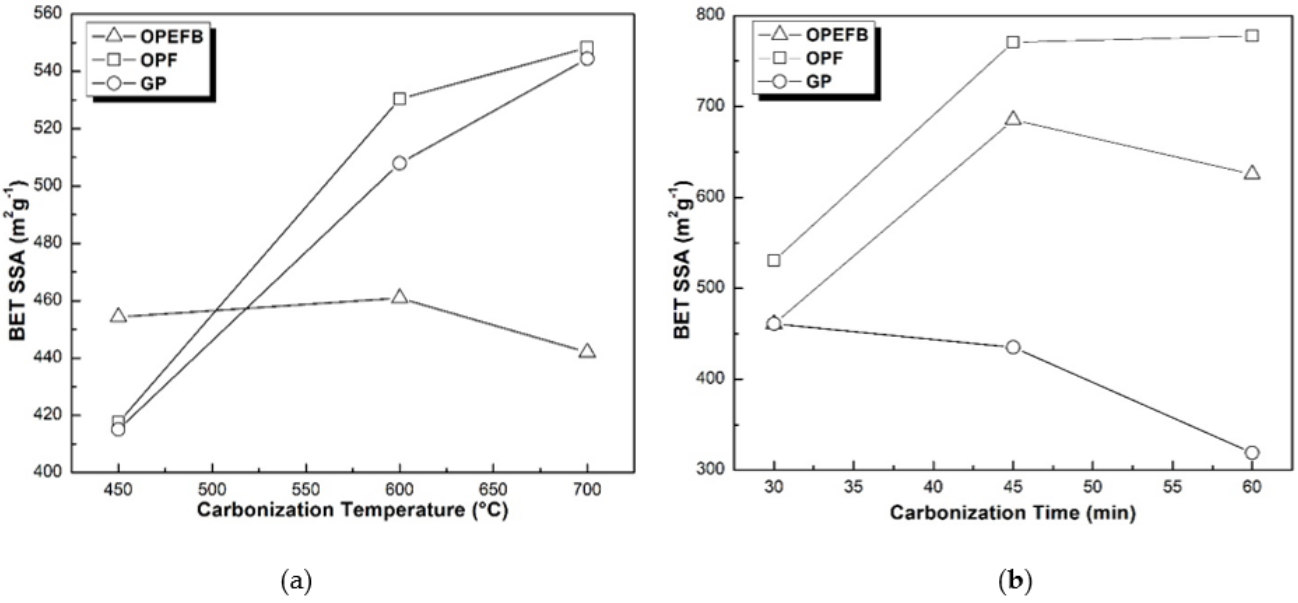

Figure 6. BET Specific Surface Area changes with (**a**) Carbonization Temperature; and (**b**) Carbonization Time.

When comparing the BET SSA of samples synthesized with different carbonization times in Figure 6b, it was observed that an increase in carbonization duration does not guarantee an increase in BET SSA. While the BET SSA of PF showed a steep increase when the carbonization time increased from 30 min to 45 min, an increase to 60 min only resulted in a slight increase in surface area. On the other hand, EFB-600-60 and GP-600-60 exhibited a lower specific surface area of 625.54 m^2g^{-1} and 319.02 m^2g^{-1}respectively compared to EFB-600-45 and GP-600-45 at 685.27 m^2g^{-1} and 435.11 m^2g^{-1}, respectively. A large specific surface area takes up a vital part in increasing the efficiency of the electro-catalyst whereby caters higher vacancy of active sites to cater to the occurrence of electrochemical reactions. Higher amount of discharge products can be stored which implied that the material exhibited high energy density [53].

Figure 7a–c shows the adsorption and desorption isotherms of the synthesized carbon samples at the carbonization temperature and time of 600 °C and 30 min. From Figure 7, all the samples exhibited type I as well as IV isotherm combination characteristics. The type I isotherm characteristics were seen within the lower relative pressure (P/P_0) range with high N_2 adsorption quantity at $P/P_0 < 0.2$. On the other hand, type IV characteristics which are represented with hysteresis loops were found within the relative pressure $0.2 < P/P_0 < 1.0$. Both the isotherms combined together had indicated that the synthesized materials contain hierarchical porous structures with micropores, mesopores, and macropores present [54]. Hierarchical porous structure is an advantageous characteristic of an efficient electrocatalyst as mesopores improves the performance of the transfer of both electrons, as well as ions, whereas micropores are responsible for the supply of a greater specific surface area which supplies more room for the storage of discharge products [55]. Besides, macropores also aid in the transport of chemical compounds, which improves the rate of reaction that takes place in the battery [56]. The hierarchical porous structure that is present within the synthesized materials can be verified with the FESEM observation shown in Figure 8.

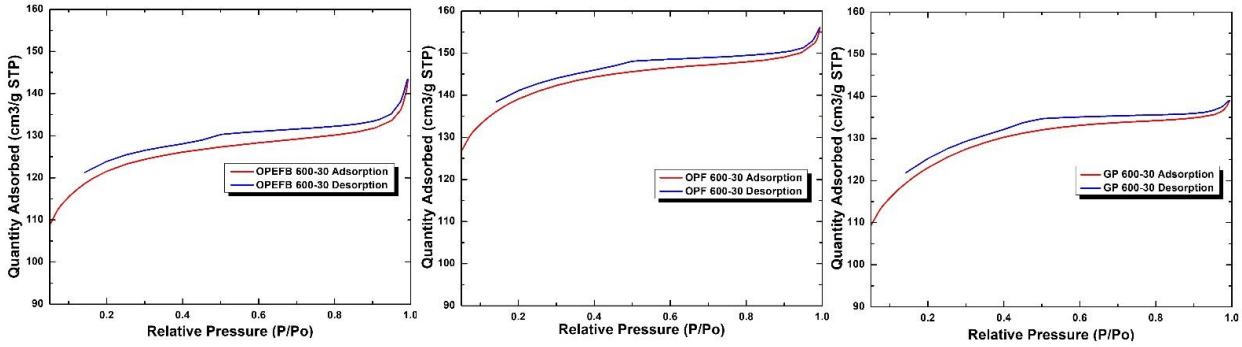

Figure 7. N_2 Adsorption-Desorption Isotherms of (**a**) EFB-600-30; (**b**) PF-600-30; and (**c**) GP-600-30.

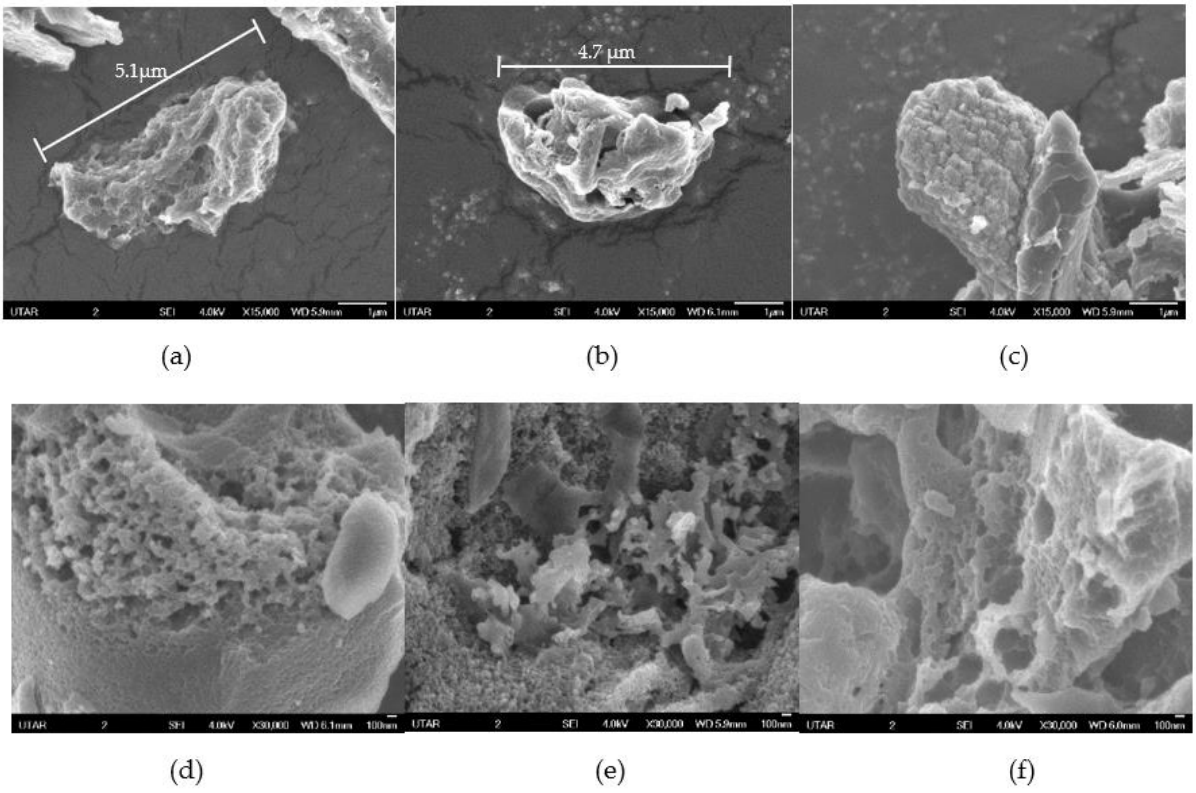

Figure 8. *Cont.*

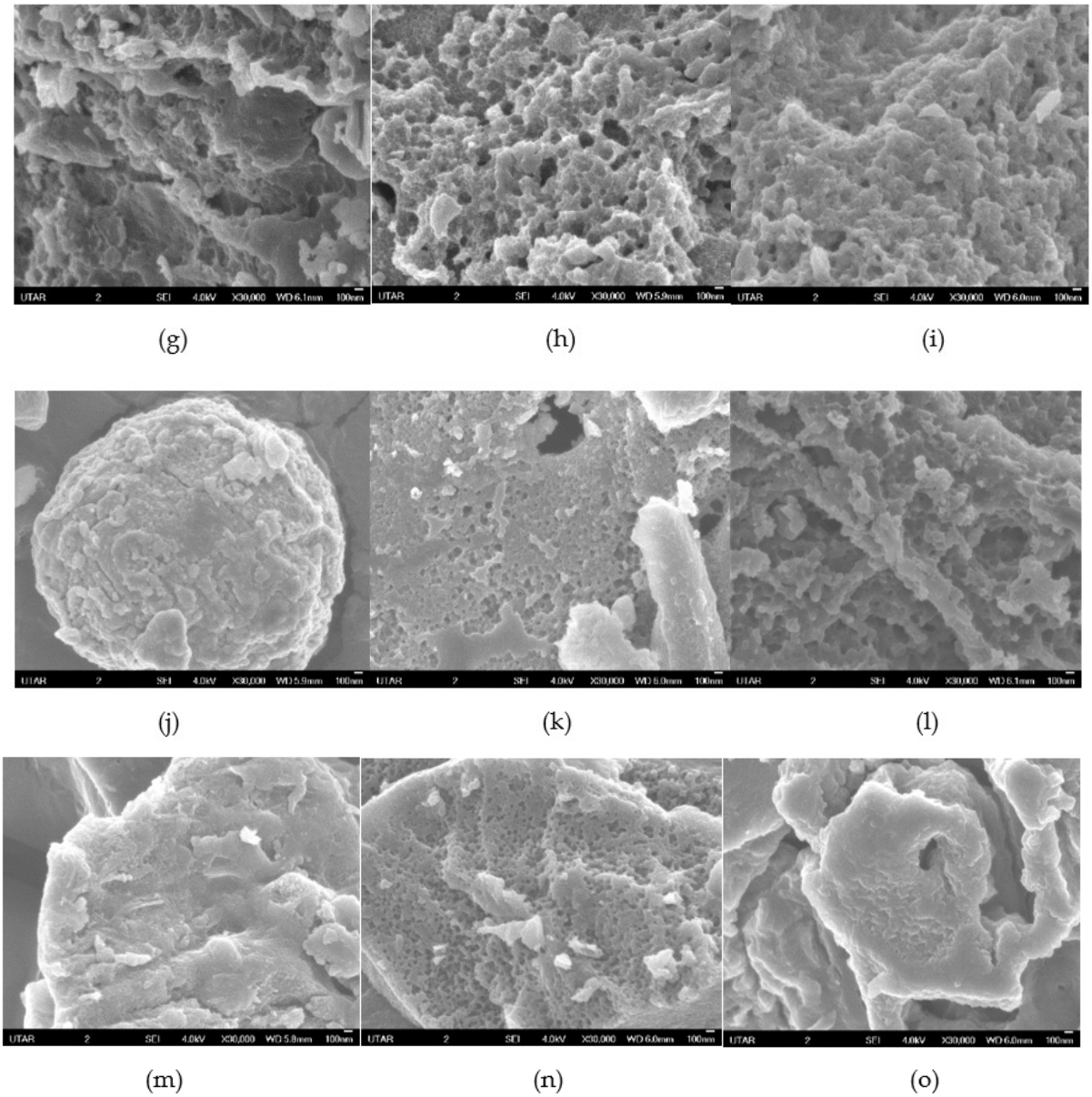

Figure 8. (**a**–**c**) EFB-450-30, PF-450-30 and GP-450-30 with 15,000 times magnification and scale of 1μm (**d**–**o**) EFB-600-30, PF-600-30, GP-600-30, EFB-700-30, PF-700-30, GP-700-30, EFB-600-45, PF-600-45, GP-600-45, EFB-600-60, PF-600-60 and GP-600-60 at 30,000 times magnification.

3.2.3. FESEM Analysis

Figure 8a–c shows EFB-450-30, PF-450-30 and GP-450 at the magnification of 15,000 times, respectively. It was observed that EFB-450-30 and PF-450-30 have achieved smaller sized particles in comparison to GP-450-30. Particles of smaller size are commonly preferred compared to bigger sized particles as it supplies more surface area with a greater number of active sites available in order for the occurrence of the electrochemical reactions. EFB-450-30 likewise had displayed more uneven surface texture compared to PF-450-30 which clarified the elevated SSA that EFB was able to achieve at carbonization temperature of 450 °C. By comparing Figure 8e,f,h, as well as Figure 8j, PF-700-30 and GP-700-30 exhibited obvious hierarchical porous structures, as well as greater structural deformity on the surface of the carbon material, in comparison to the PF and GP materials synthesized at 600 °C and 30 min. The prominent porous structure had heightened the BET SSA and hence, it was verified the elevated SSA when the carbonization temperature increased. Contrarily in

Figure 8d,g, EFB-600-30 exhibited greater porosity in comparison to EFB-700-30 which may be because of the widening of pores in the structure of the synthesized carbon from EFB when the temperature was further increased. Rios et al. found that biomasses with high lignin biomass are inclined to form macroporous structure [37].

Different precursors reacted differently to the change in carbonization time. An increase in carbonization time had resulted in producing smaller particle for EFB, as shown in Figure 8j. However in Figure 8j,m, it was observed that the surface of the OPEFB-derived carbon material particles were rougher and the porous structure reduced tremendously. Similar effect was observed for the GP-derived carbon material in Figure 8l,o whereby the pores were enlarged and less visible. By relating the surface morphology observed and the BET SSA obtained for EFB-600-45, EFB-600-60, GP-600-45 and GP-600-60, less prominent porous structure had resulted in the decrease in the SSA of the carbon material. The decrease in porosity of a carbon material could possibly be related to the thermal stability of the precursor in which the precursors were not able to withstand an elevated temperature for an extended duration. At extreme conditions, the porous structure of the material with low thermal stability collapse when the pores enlarge and the walls between pores becomes thin and weak [57,58]. According to Ornaghi et al., hemicellulose mainly attributes to the thermal stability of the lignocellulosic material, but it could not be concluded, due to the interaction between each component [59]. On the other hand, a prolonged carbonization time exhibited a positive impact on the PF-derived carbon material as its hierarchical porous structure remained intact and visible. When comparing the surface area along with the morphology of the surface of the individual material that were synthesized with respective carbonization temperatures, it can be validated that carbon materials with particles of smaller sizes as well as surfaces with immensely defective texture provided higher surface area when compared to particles with larger size and smooth texture. The hierarchical porous structure is highly desired, as the number of actives sites for reaction to take place is a function of the volume of micropores while mesopores and macropores provide channeling for ions and particles to travel which enhances the probability of occurrence of reactions [51].

Table 3 shows the comparison of the BET SSA achieved from this study with other similar studies. It can be observed that each study applied different carbonization and activation methods that produced carbon material with different SSAs despite using similar precursors. Zhang et al., had shown that a very high specific surface area of 2818 m^2g^{-1} can be achieved when the activation duration and the amount of activator added were increased [49]. From the study conducted by Bhat et al., it showed that elevated temperature itself did not necessarily result in high SSA (436.2 m^2g^{-1}) and therefore implying that activation process holds a critical part in the BET SSA elevation of a carbon material [47]. When comparing the results obtained by Bhat et al. as well as Zhang et al., the carbon material synthesized by Zhang et al. was able to achieve higher specific capacitance of 427 Fg^{-1} (0.5 Ag^{-1} current density), in comparison with Bhat et al.'s at 119.2 Fg^{-1} (0.1 Ag^{-1} current density). Despite having different current density applied, the specific capacitance of Zhang et al.'s exceeded Bhat et al.'s by several times. This indicated that the SSA of a material do affect the performance of the electro-catalyst.

According to the results obtained and observed in the previous sections, it is apparent that the change in carbonization temperature and time have different influence on the morphology of each precursor. The composition of the lignocellulosic components of each precursor is responsible for the development in porous structure as each of the component decomposes within different range of temperature in accordance with its distinctive thermal stability. For an instance, the changes in porous structure of EFB and GP were more apparent at higher carbonization temperature and longer carbonization duration, which is probably due to the complex and stretched decomposition of lignin.

By observing the characterization results in this study, it was discovered that PF possessed better potential as a raw material for the synthesis of carbon nanoparticles materials as electro-catalyst. PF had exhibited an increasing trend in BET SSA for carbonization time

and temperature. In comparison with EFB and GP, PF showed better result by achieving the highest specific surface area, due to its elevated defects in the surface structure, which does not give in to the depletion in mechanical strength when the carbonation temperature and time was increased. It is also capable of achieving a smaller particle size, which implied that nano-sized particles are feasible with further experimenting, which involves extensive synthesis parameter studies, as well as electrical conductivity tests.

Table 3. SSA comparison from this study with similar studies from the literature.

Precursor	Purpose	Synthesis Condition		SSA_{BET} (m^2/g)	Remark
		Carbonization	Activation		
Garlic Peel	Supercapacitor	1000 °C, 1 h, N_2 flow 250 mL cm^{-3}, 10 °C min^{-1}	-	436.2	[47]
Garlic Stem	ZAB	HTC 180 °C, 6 h, 900 °C, 75 min, Ar flow 100 sccm	-	991.0	[60]
Garlic Peel	Supercapacitor	600 °C, 2 h, N_2 flow 5 °C min^{-1}	4:1(KOH:C) ratio, 800 °C, 2.5 h N_2 flow 5 °C min^{-1}	2818.0	[49]
Garlic Peel	MAB	700 °C, 30 min	1:3(KOH:C) ratio, 600 °C, 30 min	541.0	This study
Empty Fruit Bunch	Wastewater treatment	900 °C, 15 min, CO_2 0.1 $Lmin^{-1}$	-	345.0	[61]
Empty Fruit Bunch	Wastewater treatment	900 °C, 15 min, Steam 2.0 mL min^{-1}	-	635.6	[61]
Empty Fruit Bunch	MAB	600 °C, 30 min	1:3(KOH:C) ratio, 600 °C, 30 min	460.9	This study
Oil Palm Frond	Wastewater treatment	500 °C, 2 h, Steam 100 cm^3 min^{-1}, 10 °C min^{-1}	-	457.7	[30]
Oil Palm Frond	MAB	700 °C, 30 min	1:3(KOH:C) ratio, 600 °C, 30 min	548.26	This study

4. Conclusions

To conclude this study, three different biomass wastes, including EFB, PF, and GP, were examined, in order to choose a good raw material in the synthesis of carbon nanoparticle as an electro-catalyst for MAB. According to the obtained results, PF was determined to be the most suitable precursor, as it was capable of achieving the highest SSA at an elevated temperature of 700 °C (548.26 m^2g^{-1}) and time of 60 min (777.62 m^2g^{-1}), due to the hierarchical porous structure and smaller particle size achieved, which are advantageous characteristics for enhancing the electrochemical efficacy of an electro-catalyst for energy storage. PF is a potential alternative to replace the current costly CNT as a material for electro-catalysts, which is greener and sustainable, yet cost-efficient. A more in-depth investigation on the electrical conductivity test will be carried out to further ascertain its potential as an electro-catalyst for MAB.

Author Contributions: Conceptualization, B.A.-L.L. and S.L.; methodology, B.A.-L.L. and S.L.; validation, Y.L.P., S.H.S. and K.H.W.; formal analysis, B.A.-L.L. and S.L.; investigation, B.A.-L.L. and S.L.; resources, S.H.S. and K.H.W.; writing—original draft preparation, B.A.-L.L. and S.L.; writing—review and editing, B.A.-L.L., S.L. and J.B.O.; supervision, S.L., Y.L.P., S.H.S. and K.H.W.; funding acquisition, S.L. and Y.L.P. All authors have read and agreed to the published version of the manuscript.

Funding: This research was fully funded by Ministry of Education, Malaysia, through the Fundamental Research Grant Scheme (FRGS/1/2018/TK10/UTAR/02/1), as well as the Universiti Tunku Abdul Rahman (UTAR) Research Grant (IPSR/RMC/UTARRF/2020-C2/W01).

Institutional Review Board Statement: Not applicable.

Informed Consent Statement: Not applicable.

Data Availability Statement: The data that was presented in this paper will be available on request from the corresponding authors.

Acknowledgments: The authors would like to express their thank to the Ministry of Education (MOE), Malaysia, for providing the Fundamental Research Grant Scheme (FRGS/1/2018/TK10/UTAR/02/1), as well as Universiti Tunku Abdul Rahman (UTAR) Research Grant (IPSR/RMC/UTARRF/2020-C2/W01) for the financial support and Universiti Tunku Abdul Rahman Research Publication Scheme (6251/S06) for the scholarship to Brenda Lim Ai-Lian.

Conflicts of Interest: The participating authors had acknowledged that there is no conflict of interest.

References

1. Praene, J.P.; Fakra, D.A.H.; Benard, F.; Ayagapin, L.; Rachadi, M.N.M. Comoros's Energy Review for Promoting Renewable Energy Sources. *Renew. Energy* **2021**, *169*, 885–893. [CrossRef]
2. Liedel, C. Sustainable Battery Materials from Biomass. *ChemSusChem* **2020**, *13*, 2110–2141. [CrossRef]
3. Mori, R. Recent Developments for Aluminum–Air Batteries. *Electrochem. Energy Rev.* **2020**, *3*, 344–369. [CrossRef]
4. Chen, T.; Jin, Y.; Lv, H.; Yang, A.; Liu, M.; Chen, B.; Xie, Y.; Chen, Q. Applications of Lithium-Ion Batteries in Grid-Scale Energy Storage Systems. *Trans. Tianjin Univ.* **2020**, *26*, 208–217. [CrossRef]
5. Clark, S.; Latz, A.; Horstmann, B. A Review of Model-Based Design Tools for Metal-Air Batteries. *Batteries* **2018**, *4*, 5. [CrossRef]
6. Wang, C.; Yu, Y.; Niu, J.; Liu, Y.; Bridges, D.; Liu, X.; Pooran, J.; Zhang, Y.; Hu, A. Recent Progress of Metal–Air Batteries-A Mini Review. *Appl. Sci.* **2019**, *9*, 2787. [CrossRef]
7. Zhong, M.; Liu, M.; Li, N.; Bu, X.H. Recent Advances and Perspectives of Metal/Covalent-Organic Frameworks in Metal-Air Batteries. *J. Energy Chem.* **2021**, *63*, 113–129. [CrossRef]
8. Lu, G.; Li, Z.; Fan, W.; Wang, M.; Yang, S.; Li, J.; Chang, Z.; Sun, H.; Liang, S.; Liu, Z. Sponge-like N-Doped Carbon Materials with Co-Based Nanoparticles Derived from Biomass as Highly Efficient Electrocatalysts for the Oxygen Reduction Reaction in Alkaline Media. *RSC Adv.* **2019**, *9*, 4843–4848. [CrossRef]
9. Ha, T.A.; Pozo-Gonzalo, C.; Nairn, K.; MacFarlane, D.R.; Forsyth, M.; Howlett, P.C. An Investigation of Commercial Carbon Air Cathode Structure in Ionic Liquid Based Sodium Oxygen Batteries. *Sci. Rep.* **2020**, *10*, 7123. [CrossRef]
10. Sathiskumar, C.; Ramakrishnan, S.; Vinothkannan, M.; Kim, A.R.; Karthikeyan, S.; Yoo, D.J. Nitrogen-Doped Porous Carbon Derived from Biomass Used as Trifunctional Electrocatalyst toward Oxygen Reduction, Ox-ygen Evolution and Hydrogen Evolution Reactions. *Nanomaterials* **2020**, *10*, 76. [CrossRef] [PubMed]
11. Sekhon, S.S.; Lee, J.; Park, J.S. Biomass-Derived Bifunctional Electrocatalysts for Oxygen Reduction and Evolution Reaction: A Review. *J. Energy Chem.* **2021**, *65*, 149–172. [CrossRef]
12. Malik, S.; Marchesan, S. Growth, Properties, and Applications of Branched Carbon Nanostructures. *Nanomaterials* **2021**, *11*, 2728. [CrossRef] [PubMed]
13. Gopalakrishnan, A.; Badhulika, S. Effect of Self-Doped Heteroatoms on the Performance of Biomass-Derived Carbon for Supercapacitor Applications. *J. Power Sources* **2020**, *480*, 228830. [CrossRef]
14. He, G.; Yan, G.; Song, Y.; Wang, L. Biomass Juncus Derived Nitrogen-Doped Porous Carbon Materials for Supercapacitor and Oxygen Reduction Reaction. *Front. Chem.* **2020**, *8*, 226. [CrossRef] [PubMed]
15. Hu, W.; Xiang, R.; Lin, J.; Cheng, Y.; Lu, C. Lignocellulosic Biomass-Derived Carbon Electrodes for Flexible Supercapacitors: An Overview. *Materials* **2021**, *14*, 4571. [CrossRef]
16. Wang, N.; Li, T.; Song, Y.; Liu, J.; Wang, F. Metal-Free Nitrogen-Doped Porous Carbons Derived from Pomelo Peel Treated by Hypersaline Environments for Oxygen Reduction Reaction. *Carbon* **2018**, *130*, 692–700. [CrossRef]
17. Baruah, J.; Nath, B.K.; Sharma, R.; Kumar, S.; Deka, R.C.; Baruah, D.C.; Kalita, E. Recent Trends in the Pretreatment of Lignocellulosic Biomass for Value-Added Products. *Front. Energy Res.* **2018**, *6*, 141. [CrossRef]
18. Kolanowski, L.; Graś, M.; Bartkowiak, M.; Doczekalska, B.; Lota, G. Electrochemical Capacitors Based on Electrodes Made of Lignocellulosic Waste Materials. *Waste Biomass Valorization* **2020**, *11*, 3863–3871. [CrossRef]
19. Hendriansyah, R.; Prakoso, T.; Widiatmoko, P.; Nurdin, I.; Devianto, H. Manufacturing Carbon Material by Carbonization of Cellulosic Palm Oil Waste for Supercapacitor Material. *MATEC Web Conf.* **2018**, *156*, 03018. [CrossRef]
20. Han, J.; Lee, J.H.; Roh, K.C. Herbaceous Biomass Waste-Derived Activated Carbons for Supercapacitors. *J. Electrochem. Sci. Technol.* **2018**, *9*, 157–162. [CrossRef]
21. Elmouwahidi, A.; Bailón-García, E.; Pérez-Cadenas, A.F.; Maldonado-Hódar, F.J.; Carrasco-Marín, F. Activated Carbons from KOH and H_3PO_4-Activation of Olive Residues and Its Application as Supercapacitor Electrodes. *Electrochim. Acta* **2017**, *229*, 219–228. [CrossRef]
22. Kim, M.J.; Park, J.E.; Kim, S.; Lim, M.S.; Jin, A.; Kim, O.H.; Kim, M.J.; Lee, K.S.; Kim, J.; Kim, S.S.; et al. Biomass-Derived Air Cathode Materials: Pore-Controlled S,N-Co-Doped Carbon for Fuel Cells and Metal–Air Batteries. *ACS Catal.* **2019**, *9*, 3389–3398. [CrossRef]

23. Hao, X.; Chen, W.; Jiang, Z.; Tian, X.; Hao, X.; Maiyalagan, T.; Jiang, Z.J. Conversion of Maize Straw into Nitrogen-Doped Porous Graphitized Carbon with Ultra-High Surface Area as Excellent Oxygen Reduction Electrocatalyst for Flexible Zinc–Air Batteries. *Electrochim. Acta* **2020**, *362*, 137143. [CrossRef]
24. Zainol, M.M.; Amin, N.A.S.; Asmadi, M. Preparation and Characterization of Impregnated Magnetic Particles on Oil Palm Frond Activated Carbon for Metal Ions Removal. *Sains Malays.* **2017**, *46*, 773–782. [CrossRef]
25. Muhamad, N.A.S.; Hanoin, M.A.H.M.; Mokhtar, N.M.; Lau, W.J.; Jaafar, J. Industrial Application of Membrane Distillation Technology Using Palm Oil Mill Effluent in Malaysia. *Mater. Today Proc.* **2021**, 575. [CrossRef]
26. Nurika, I.; Shabrina, E.N.; Azizah, N.; Suhartini, S.; Bugg, T.D.H.; Barker, G.C. Application of Ligninolytic Bacteria to the Enhancement of Lignocellulose Breakdown and Methane Production from Oil Palm Empty Fruit Bunches (OPEFB). *Bioresour. Technol. Rep.* **2022**, *17*, 100951. [CrossRef]
27. Mahmud, M.S.; Chong, K.P. Formulation of Biofertilizers from Oil Palm Empty Fruit Bunches and Plant Growth-Promoting Microbes: A Comprehensive and Novel Approach towards Plant Health. *J. King Saud Univ.-Sci.* **2021**, *33*, 101647. [CrossRef]
28. Fatihah Salleh, S.; Abd Rahman, A.; Ab Rashid Tuan Abdullah, T. Potential of Deploying Empty Fruit Bunch (EFB) for Biomass Cofiring in Malaysia's Largest Coal Power Plant. In Proceedings of the 2018 IEEE International Conference on Power and Energy (PECon2018), Kuala Lumpur, Malaysia, 3–4 December 2018.
29. Department of Statistics Malaysia Malaysian CPI Inflation Calculator. Available online: https://www.dosm.gov.my/cpi_calc/ (accessed on 22 December 2021).
30. Lawal, A.A.; Hassan, M.A.; Farid, M.A.A.; Yasim-Anuar, T.A.T.; Yusoff, M.Z.M.; Zakaria, M.R.; Roslan, A.M.; Mokhtar, M.N.; Shirai, Y. Production of Biochar from Oil Palm Frond by Steam Pyrolysis for Removal of Residual Contaminants in Palm Oil Mill Effluent Final Discharge. *J. Clean. Prod.* **2020**, *265*, 121643. [CrossRef]
31. Osman, N.B.; Shamsuddin, N.; Uemura, Y. Activated Carbon of Oil Palm Empty Fruit Bunch (EFB); Core and Shaggy. *Procedia Eng.* **2016**, *148*, 758–764. [CrossRef]
32. Zeng Wei, H. Effect of Pretreatment for Synthesis of Oil Palm Frond Based Catalyst for Biodiesel Production. Ph.D. Thesis, Universiti Tunku Abdul Rahman, Kampar, Perak, Malaysia, May 2019.
33. Rodríguez-Solana, R.; Salgado, J.M.; Domínguez, J.M.; Cortés-Diéguez, S. Characterization of Fennel Extracts and Quantification of Estragole: Optimization and Comparison of Accelerated Solvent Extraction and Soxhlet Techniques. *Ind. Crops Prod.* **2014**, *52*, 528–536. [CrossRef]
34. Sluiter, A.; Ruiz, R.; Scarlata, C.; Sluiter, J.; Templeton, D. Determination of Extractives in Biomass: Laboratory Analytical Procedure (LAP). 2008. Available online: https://www.nrel.gov/docs/gen/fy08/42619.pdf (accessed on 19 December 2021).
35. Chin, D.W.K.; Lim, S.; Pang, Y.L.; Lim, C.H.; Shuit, S.H.; Lee, K.M.; Chong, C.T. Effects of Organic Solvents on the Organosolv Pretreatment of Degraded Empty Fruit Bunch for Fractionation and Lignin Removal. *Sustainability* **2021**, *13*, 6757. [CrossRef]
36. Wang, Y.J.; Fang, B.; Zhang, D.; Li, A.; Wilkinson, D.P.; Ignaszak, A.; Zhang, L.; Zhang, J. *A Review of Carbon-Composited Materials as Air-Electrode Bifunctional Electrocatalysts for Metal-Air Batteries*; Springer: Singapore, 2018; Volume 1, ISBN 0123456789.
37. Del Mar Saavedra Rios, C.; Simone, V.; Simonin, L.; Martinet, S.; Dupont, C. Biochars from Various Biomass Types as Precursors for Hard Carbon Anodes in Sodium-Ion Batteries. *Biomass Bioenergy* **2018**, *117*, 32–37. [CrossRef]
38. Chen, S.; Xia, Y.; Zhang, B.; Chen, H.; Chen, G.; Tang, S. Disassembly of Lignocellulose into Cellulose, Hemicellulose, and Lignin for Preparation of Porous Carbon Materials with Enhanced Performances. *J. Hazard. Mater.* **2021**, *408*, 124956. [CrossRef] [PubMed]
39. Leng, L.; Xiong, Q.; Yang, L.; Li, H.; Zhou, Y.; Zhang, W.; Jiang, S.; Li, H.; Huang, H. An Overview on Engineering the Surface Area and Porosity of Biochar. *Sci. Total Environ.* **2021**, *763*, 144204. [CrossRef] [PubMed]
40. Hendrawan, Y.; Sajidah, N.; Umam, C.; Fauzy, M.R.; Wibisono, Y.; Hawa, L.C. Effect of Carbonization Temperature Variations and Activator Agent Types on Activated Carbon Characteristics of Sengon Wood Waste (*Paraserianthes Falcataria* (L.) *Nielsen*). In Proceedings of the 12th International Interdisciplinary Studies Seminar—Environmental Conservation and Education for Sustainable Development, Malang, Indonesia, 14–15 November 2018; IOP Publishing: Bristol, UK, 2019; Volume 239.
41. Zhao, R.; Ni, B.; Wu, L.; Sun, P.; Chen, T. Carbon-Based Iron-Cobalt Phosphate FeCoP/C as an Effective ORR/OER/HER Triunctional Electrocatalyst. *Colloids Surf. A Physicochem. Eng. Asp.* **2022**, *635*, 128118. [CrossRef]
42. Oh, W.-D.; Lisak, G.; Webster, R.D.; Liang, Y.N.; Veksha, A.; Giannis, A.; Moo, J.G.S.; Lim, J.W.; Lim, T.T. Insights into the Thermolytic Transformation of Lignocellulosic Biomass Waste to Redox-Active Carbocatalyst: Durability of Surface Active Sites. *Appl. Catal. B Environ.* **2018**, *233*, 120–129. [CrossRef]
43. Zhao, L.; Ning, G.; Zhang, S. Green Synthesis of S-Doped Carbon Nanotubes via Gaseous Post-Treatment and Their Application as Conductive Additive in Li Ion Batteries. *Carbon* **2021**, *179*, 425–434. [CrossRef]
44. Babinszki, B.; Jakab, E.; Terjék, V.; Sebestyén, Z.; Várhegyi, G.; May, Z.; Mahakhant, A.; Attanatho, L.; Suemanotham, A.; Thanmongkhon, Y.; et al. Thermal Decomposition of Biomass Wastes Derived from Palm Oil Production. *J. Anal. Appl. Pyrolysis* **2021**, *155*, 105069. [CrossRef]
45. Sunphorka, S.; Chalermsinsuwan, B.; Piumsomboon, P. Artificial Neural Network Model for the Prediction of Kinetic Parameters of Biomass Pyrolysis from Its Constituents. *Fuel* **2017**, *193*, 142–158. [CrossRef]
46. Xu, C.A.; Qu, Z.; Meng, H.; Chen, B.; Wu, X.; Cui, X.; Wang, K.; Wu, K.; Shi, J.; Lu, M. Effect of Polydopamine-Modified Multi-Walled Carbon Nanotubes on the Thermal Stability and Conductivity of UV-Curable Polyurethane/Polysiloxane Pressure-Sensitive Adhesives. *Polymer* **2021**, *223*, 123615. [CrossRef]

47. Bhat, V.S.; Kanagavalli, P.; Sriram, G.; B, R.P.; John, N.S.; Veerapandian, M.; Kurkuri, M.; Hegde, G. Low Cost, Catalyst Free, High Performance Supercapacitors Based on Porous Nano Carbon Derived from Agriculture Waste. *J. Energy Storage* **2020**, *32*, 101829. [CrossRef]
48. Li, J.; Dou, B.; Zhang, H.; Zhang, H.; Chen, H.; Xu, Y. Thermochemical Characteristics and Non-Isothermal Kinetics of Camphor Biomass Waste. *J. Environ. Chem. Eng.* **2021**, *9*. [CrossRef]
49. Zhang, Q.; Han, K.; Li, S.; Li, M.; Li, J.; Ren, K. Synthesis of Garlic Skin-Derived 3D Hierarchical Porous Carbon for High-Performance Supercapacitors. *Nanoscale* **2018**, *10*, 2427–2437. [CrossRef] [PubMed]
50. Zhao, C.; Liu, G.; Sun, N.; Zhang, X.; Wang, G.; Zhang, Y.; Zhang, H.; Zhao, H. Biomass-Derived N-Doped Porous Carbon as Electrode Materials for Zn-Air Battery Powered Capacitive Deionization. *Chem. Eng. J.* **2018**, *334*, 1270–1280. [CrossRef]
51. Chakraborty, I.; Sathe, S.M.; Dubey, B.K.; Ghangrekar, M.M. Waste-Derived Biochar: Applications and Future Perspective in Microbial Fuel Cells. *Bioresour. Technol.* **2020**, *312*, 123587. [CrossRef]
52. Xie, Y.; Feng, C.; Guo, Y.; Hassan, A.; Li, S.; Zhang, Y.; Wang, J. Dimethylimidazole and Dicyandiamide Assisted Synthesized Rich-Defect and Highly Dispersed CuCo-N_x Anchored Hollow Graphite Carbon Nanocages as Efficient Trifunctional Electrocatalyst in the Same Electrolyte. *J. Power Sources* **2022**, *517*, 230721. [CrossRef]
53. Chen, W.; Gong, Y.F.; Liu, J.H. Recent Advances in Electrocatalysts for Non-Aqueous Li–O_2 Batteries. *Chin. Chem. Lett.* **2017**, *28*, 709–718. [CrossRef]
54. Peng, L.; Liang, Y.; Dong, H.; Hu, H.; Zhao, X.; Cai, Y.; Xiao, Y.; Liu, Y.; Zheng, M. Super-Hierarchical Porous Carbons Derived from Mixed Biomass Wastes by a Stepwise Removal Strategy for High-Performance Supercapacitors. *J. Power Sources* **2018**, *377*, 151–160. [CrossRef]
55. Lei, W.; Deng, Y.P.; Li, G.; Cano, Z.P.; Wang, X.; Luo, D.; Liu, Y.; Wang, D.; Chen, Z. Two-Dimensional Phosphorus-Doped Carbon Nanosheets with Tunable Porosity for Oxygen Reactions in Zinc-Air Batteries. *ACS Catal.* **2018**, *8*, 2464–2472. [CrossRef]
56. Seow, Y.X.; Tan, Y.H.; Mubarak, N.M.; Kansedo, J.; Khalid, M.; Ibrahim, M.L.; Ghasemi, M. A Review on Biochar Production from Different Biomass Wastes by Recent Carbonization Technologies and Its Sustainable Applications. *J. Environ. Chem. Eng.* **2022**, *10*, 107017. [CrossRef]
57. Ahmad, M.A.; Herawan, S.G.; Yusof, A.A. Effect of Activation Time on the Pinang Frond Based Activated Carbon for Remazol Brilliant Blue R Removal. *J. Mech. Eng. Sci.* **2014**, *7*, 1085–1093. [CrossRef]
58. Fu, Y.; Shen, Y.; Zhang, Z.; Ge, X.; Chen, M. Activated Bio-Chars Derived from Rice Husk via One- and Two-Step KOH-Catalyzed Pyrolysis for Phenol Adsorption. *Sci. Total Environ.* **2019**, *646*, 1567–1577. [CrossRef] [PubMed]
59. Ornaghi, H.L.; Ornaghi, F.G.; Neves, R.M.; Monticeli, F.; Bianchi, O. Mechanisms Involved in Thermal Degradation of Lignocellulosic Fibers: A Survey Based on Chemical Composition. *Cellulose* **2020**, *27*, 4949–4961. [CrossRef]
60. Ma, Z.; Wang, K.; Qiu, Y.; Liu, X.; Cao, C.; Feng, Y.; Hu, P.A. Nitrogen and Sulfur Co-Doped Porous Carbon Derived from Bio-Waste as a Promising Electrocatalyst for Zinc-Air Battery. *Energy* **2018**, *143*, 43–55. [CrossRef]
61. Amosa, M.K.; Jami, M.S.; AlKhatib, M.F.R.; Jimat, D.N.; Muyibi, S.A. Comparative and Optimization Studies of Adsorptive Strengths of Activated Carbons Produced from Steam- and CO_2-Activation for BPOME Treatment. *Adv. Environ. Biol.* **2014**, *8*, 603–612.